Supporting Information for

# Ring fusion in tetrathienylethene cored perylene diimide tetramers affords acceptors with strong and broad absorption in the near-UV to visible region

Qiao He,‡[a] Flurin D. Eisner,‡[b] Drew Pearce,[b] Thomas Hodsden,[a] Elham Rezasoltani,[b] Daniel Medranda,[b] Zhuping Fei,[c] Jenny Nelson,*[b] and Martin Heeney*[a]

[a]*Department of Chemistry and Centre for Processable Electronics, Imperial College London, London W12 0BZ, UK. E-mail: m.heeney@imperial.ac.uk*
[b]*Department of Physics and Centre for Processable Electronics, Imperial College London, London SW7 2AZ, UK. E-mail: jenny.nelson@imperial.ac.uk*
[c]*Institute of Molecular Plus, Tianjin Key Laboratory of Molecular Optoelectronic Science, Tianjin University, Tianjin 300072, P. R. China*

**General Procedures.** PTB7-Th was purchased from Solarmer Material Inc. PffBT4T-2OD, PBDB-T, PFBDB-T and P4FBDB-T were synthesized according to the pervious report.[1-4] All reactions were carried out in oven-dried glassware under nitrogen using solvents and reagents as commercially supplied, unless otherwise stated. $^{1}H$ and $^{13}C$ NMR spectra were recorded on a Bruker AV-400 (400 MHz) NMR spectrometer, using the residual solvent resonance of $CDCl_3$. Chemical shifts are reported in parts per million (ppm, δ). GC-MS was carried out on an Agilent GC 7890A and MS 5975C. Matrix-assisted laser desorption/ionization time-of-flight (MALDI-TOF) mass spectrometry was performed on a Bruker ultrafleXtreme MALDI-TOF analyzer, matrix: DCTB in THF, 10 mg $mL^{-1}$. Preparative recycling GPC was run at room temperature using chloroform as eluent. The system consisted of a high pressure liquid chromatography apparatus (JAI LaboACE LC-5060 series) equipped with a pump (P-LA60, flow rate 10 ml $min^{-1}$), a UV detector (UV-VIS4ch LA, λ = 210 nm, 254 nm, 330 nm, 400 nm) and two columns (Jaigel 2HR and 2.5HR, inner diameter 20 mm × length 600 mm each).

**Theoretical calculations.** Density functional theory (DFT) calculations were modeled using Gaussian at the B3LYP/6-31G* level. The side chains were modified to methyl groups to simplify the calculations.[5-7] For the TD-DFT calculations the structures were first reoptimised at the slightly larger basis set 6-311g then TD-DFT was used to calculate the first 100 excited states which were then broadened with a half-width at half-height of 0.2 eV to produce the extinction coefficients. Frequency calculations were also performed to calculate the vibrational transitions.

**Thermal analysis.** Thermogravimetric analysis (TGA) was carried out using a Shimadzu thermogravimetric analyzer (model DTG-60, with heating from 25 to 600 °C at a heating rate of 10 °C $min^{-1}$ under nitrogen. Differential scanning calorimetry (DSC) measurements were performed using a Mettler differential scanning calorimeter (DSC822e) at a scanning speed of 10 °C $min^{-1}$ from 20 to 280 °C under nitrogen.

**Optical and electrochemical characterizations.** UV-Vis absorption spectra were recorded on a UV-1601 Shimadzu UV-Vis spectrometer. Solution samples were prepared by dissolving the two small molecules TTE-PDI4 and FTTE-PDI4 in chloroform with the concentration of $1.0 \times 10^{-5}$ M and film samples were spin-cast on quartz plates. Electrochemical measurements were carried out under nitrogen with a deoxygenated solution of tetra-n-butylammonium hexafluorophosphate (0.1 M) in $CH_3CN$ using a computer-controlled CHI660C electrochemical workstation, a platinum plate working electrode, a platinum-wire auxiliary electrode, and Ag/AgCl as a reference electrode. Samples were drop-cast onto the working electrode to form thin films and potentials were referenced to ferrocenium/ferrocene ($FeCp_2^{+/0}$) couple by using ferrocene as an internal standard. The scan rate is 100 mV $s^{-1}$.

**Morphology analysis.** Atomic force microscopy (AFM) images were obtained with a Picoscan PicoSPM LE scanning probe in tapping mode. Samples were spin-cast on ITO/ZnO substrates. X-ray diffraction (XRD) measurements were performed on Bruker D2 Phaser.

**Solar cell fabrication and testing.** Organic solar cell devices were fabricated onto pre-patterned ITO covered glass substrates with the device architecture ITO/ZnO/Active layer/$MoO_3$/Ag. After sequential cleaning of the ITO with the detergent (Decon 90), acetone and isopropyl alcohol, a zinc acetate dihydrate precursor solution (219.5 mg in the mixture of 2 mL 2-methoxyethanol and 60 μL monoethanolamine) was spin coated and was annealed at 200 °C for 1 h. Active layers are blend films dissolved in chlorobenzene with a concentration of 20 mg $ml^{-1}$ using PTB7-Th, PffBT4T-2OD, PBDB-T, PFBDB-T or P4FBDB-T as the donor, and TTE-PDI4 or FTTE-PDI4 as the acceptor. The blend solutions were preheated and then spin coated onto the ZnO coated ITO substrate and the thicknesses of the active layers were ~80-100 nm. The active layers were used as-spun or treated with thermal annealing. 1-Chloronaphthalene (CN) was used as solvent additive to improve the blend morphology of active layers. To complete the devices, $MoO_3$ (*ca.* 10 nm) and Ag (*ca.* 80 nm) were evaporated sequentially under high vacuum (*ca.* $10^{-5}$ Pa) under shadow masks to fabricate devices with an area of 5 $mm^2$. Current-voltage characteristics were measured with a Keithley 236 source/measure unit under AM 1.5 solar illumination (Oriel 300 W solar simulator) at an intensity of 100 mW $cm^{-2}$. All electrical measurements of OPVs were executed in the inert nitrogen purged devices chamber.

**EQE measurements.** External quantum efficiency (EQE) was measured by a 100 W tungsten

halogen lamp (Bentham IL1 with Bentham 605 stabilized current power supply) coupled to a monochromator with computer-controlled stepper motor (Bentham M300, 300 mm focal length, slit width 3.7 nm, 1800 lines/m grating) The photon flux of light incident on the samples was calibrated using a UV-enhanced silicon photodiode. A 590 nm long-pass glass filter was inserted into the beam at illumination wavelengths longer than 620 nm to remove light from second-order diffraction. Measurement duration for a given wavelength was sufficient to ensure the current had stabilized.

**Luminescence Measurements**

Luminscence measurements were performed with a Shamrock 303 spectrograph together with an iDUS InGaAs array detector cooled to -90 °C. The intensity of the spectra was calibrated using the spectrum from a calibrated halogen lamp. PL measurements were performed using the excitation from a 473 nm diode laser.

**Synthesis of DTK.** To a solution of thiophene (5.05 g, 60 mmol) in anhydrous THF (30 mL) at −78 °C was added a solution of n-BuLi (24 mL of a 2.5 M solution in hexane, 60 mmol) dropwise. After the resulting mixture was stirred for 1 h at this temperature, dimethylcarbamyl chloride (3.23 g, 30 mmol) was added in one portion. The mixture was stirred for 30 min and then allowed to warm to room temperature for 2 h. The reaction was quenched with aqueous HCl (1 M, 30 mL) and the mixture was extracted with diethyl ether (3 × 30 mL). The combined organic layers were dried over $MgSO_4$ and concentrated under reduced pressure. The residue was purified by silica gel chromatography (eluent: dichloromethane (DCM)) to afford a pale yellow solid (4.87 g, yield 83.5%). $^1$H NMR ($CDCl_3$, 400 MHz): $\delta$ 7.89 (d, $J$ = 3.8 Hz, 2H), 7.70 (d, $J$ = 5.0 Hz, 2H), 7.18 (dd, $J$ = 3.7, 4.6 Hz, 2H). $^{13}$C NMR ($CDCl_3$, 100 MHz): $\delta$ 178.56, 142.65, 133.49, 133.09, 127.99. MS (EI, GC-MS) m/z = 194 ($M^+$).

**Synthesis of TTE.** To anhydrous THF (150 mL) was added titanium(IV) chloride (5 g, 26.4 mmol) in one portion at 0 °C. After being stirred for 30 min at this temperature, activated zinc powder (3.76 g, 57.6 mmol) and pyridine (2.2 mL, 26.4 mmol) were added, and then the mixture was warmed to room temperature for 2 h. A solution of DTK (4.66 g, 24 mmol) in THF (20 mL) was added and the reaction was heated for 20 h at 80 °C. After being cooled to room temperature, an aqueous saturated solution of $Na_2CO_3$ (30 mL) was added to quench the reaction and the mixture was passed through a silica gel plug (eluent: DCM). The mixture was further extracted with DCM and dried over $MgSO_4$. The solvent was removed under reduced pressure, and the residue was purified by silica gel chromatography (eluent: DCM/petroleum ether = 1/3) and recrystallization from chloroform/ethanol to afford an orange solid (1.28 g, yield 30%). $^1$H NMR ($CDCl_3$, 400 MHz): $\delta$ 7.32 (dd, $J$ = 5.1, 1.2 Hz, 4H), 6.94 (dd, $J$ = 5.1, 3.6 Hz, 4H), 6.88 (dd, $J$ = 3.7, 1.2 Hz, 4H). $^{13}$C NMR ($CDCl_3$, 100 MHz): $\delta$ 144.37, 130.13, 127.87, 127.77, 126.77. MS (MALDI-TOF) m/z = 356.7 ($M^+$).

**Synthesis of TTE-Bpin4.** A mixture of TTE (815 mg, 2.28 mmol), bis(pinacolato)diboron (3.48 g, 13.7 mmol), 4,4'-di-tert-butyl-2,2'-dipyridyl (171.8 mg, 0.64 mmol) and $[Ir(OMe)Cod]_2$ (84.8 mg, 0.128 mmol) in anhydrous hexane (40 ml) was heated at 80 °C for 36 hours. After being cooled to room temperature, the mixture was poured into brine (30 mL) and extracted with DCM (3 × 30 mL). The combined organic layer was dried by $MgSO_4$ and concentrated under reduced pressure. The residue was purified by recrystallization from DCM/methanol to afford an orange solid (890 mg, yield 45.2%). $^1$H NMR ($CDCl_3$, 400 MHz): $\delta$ 7.36 (d, $J$ = 3.6 Hz, 4H), 6.87 (d, $J$ = 3.6 Hz, 4H), 1.31 (s, 48H). $^{13}$C NMR ($CDCl_3$, 100 MHz): $\delta$ 151.78, 137.07, 130.89, 128.78, 84.22, 24.96. MS (MALDI-TOF) m/z = 860.48 ($M^+$).

Synthesis of **TTE-PDI4**. To a mixture of TTE-Bpin4 (120 mg, 0.14 mmol), PDI-Br (480 mg, 0.58 mmol), $Pd_2(dba)_3$ (25.6 mg, 0.028 mmol) and SPhos (114.5 mg, 0.28 mmol), tetrahydrofuran (12 mL) and 2M $K_2CO_3$ aqueous solution (4 mL) was added. The reaction was refluxed for 15 h and then cooled to room temperature. The mixture was poured into water (30 mL) and extracted with chloroform (3 × 30 mL). The combined organic layer was dried over $MgSO_4$ and concentrated under reduced pressure. The residue was purified by silica gel chromatography (eluent chloroform/petroleum ether = 3/1), followed by further purification by recycling preparative GPC (eluent: chloroform), to afford a dark red solid (190 mg, yield 40%). $^1$H NMR ($CDCl_3$, 400 MHz): $\delta$ 8.74-7.96 (m, 30H), 7.39-7.01 (m, 6H), 5.23-4.75 (br, 8H), 2.32-1.46 (br, 32H), 1.46-0.92 (br, 128H), 0.92-0.57 (m, 48H). $^{13}$C NMR ($CDCl_3$, 100 MHz): $\delta$ 165.27, 164.18, 163.84, 147.05, 135.12, 134.36, 133.94, 133.05, 129.64, 129.21, 128.21, 127.62, 127.14, 123.73, 122.96, 54.90, 32.46, 32.23, 31.87, 31.80, 29.34, 29.21, 27.04, 26.91, 22.73, 22.69, 14.19. MS (MALDI-TOF) m/z = 3369.0 ($M^+$).

Synthesis of **FTTE-PDI4**.

To a solution of TTE-PDI4 (120 mg, 0.0356 mmol) in anhydrous toluene (20 mL), $FeCl_3$ (577 mg, 3.56 mmol) in $CH_3NO_2$ (2 mL) was added. After being heated to reflux for 3 h, the mixture was poured into water (30 mL) and extracted with chloroform (3 × 30 mL). The combined organic layer was dried over $MgSO_4$ and the solvent was removed under reduced pressure. The crude product was purified by silica gel chromatography (eluent chloroform/petroleum ether = 3/1), followed by further purification by recycling preparative GPC (eluent: chloroform), to afford a dark red solid (75 mg, yield 62.6%). $^1$H NMR ($C_2D_2Cl_4$, 120 °C, 400 MHz): $\delta$ 10.68 (br, 4H), 9.46 (d, $J$ = 8.1 Hz, 4H), 9.40-9.29 (m, 8H), 9.28-9.24 (br, 4H), 9.16-9.08 (br, 2H), 8.91 (d, $J$ = 8.1 Hz, 4H), 5.70-5.59 (br, 4H), 4.45-4.31 (br, 4H), 2.75-0.56 (m, 208H). $^{13}$C NMR ($CDCl_3$, 100 MHz): $\delta$ 164.32, 163.98, 163.15, 140.39, 137.06, 133.40, 132.72, 130.34, 128.98, 128.40, 126.50, 126.05, 125.13, 124.57, 124.31, 123.91, 123.81, 123.41, 55.71, 32.95, 32.11, 31.68, 29.62, 28.99, 27.52, 27.40, 26.52, 22.88, 22.43, 14.56, 14.31, 13.92. MS (MALDI-TOF) m/z = 3360.6 ($M^+$).

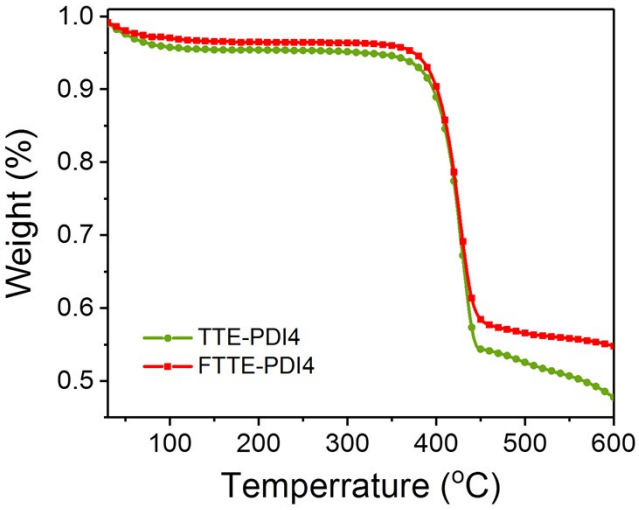


Fig. S1 TGA curves of TTE-PDI4 and FTTE-PDI4 at a heating speed of 10 °C $min^{-1}$ under nitrogen ($T_d$ at 5% weight loss).

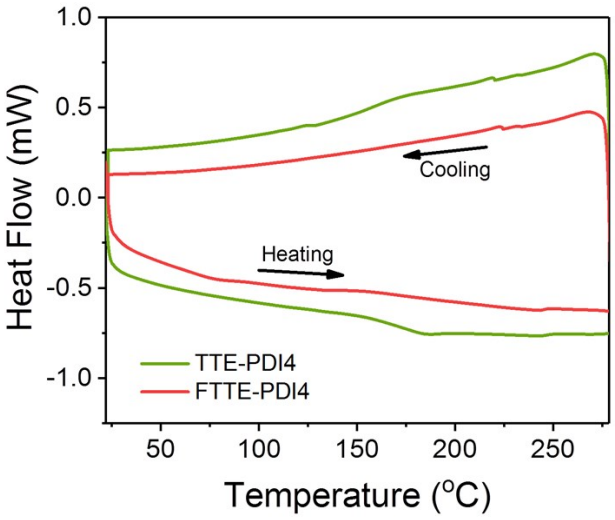


Fig. S2 DSC curves of TTE-PDI4 and FTTE-PDI4 at a heating/cooling speed of 10 °C $min^{-1}$ under nitrogen.

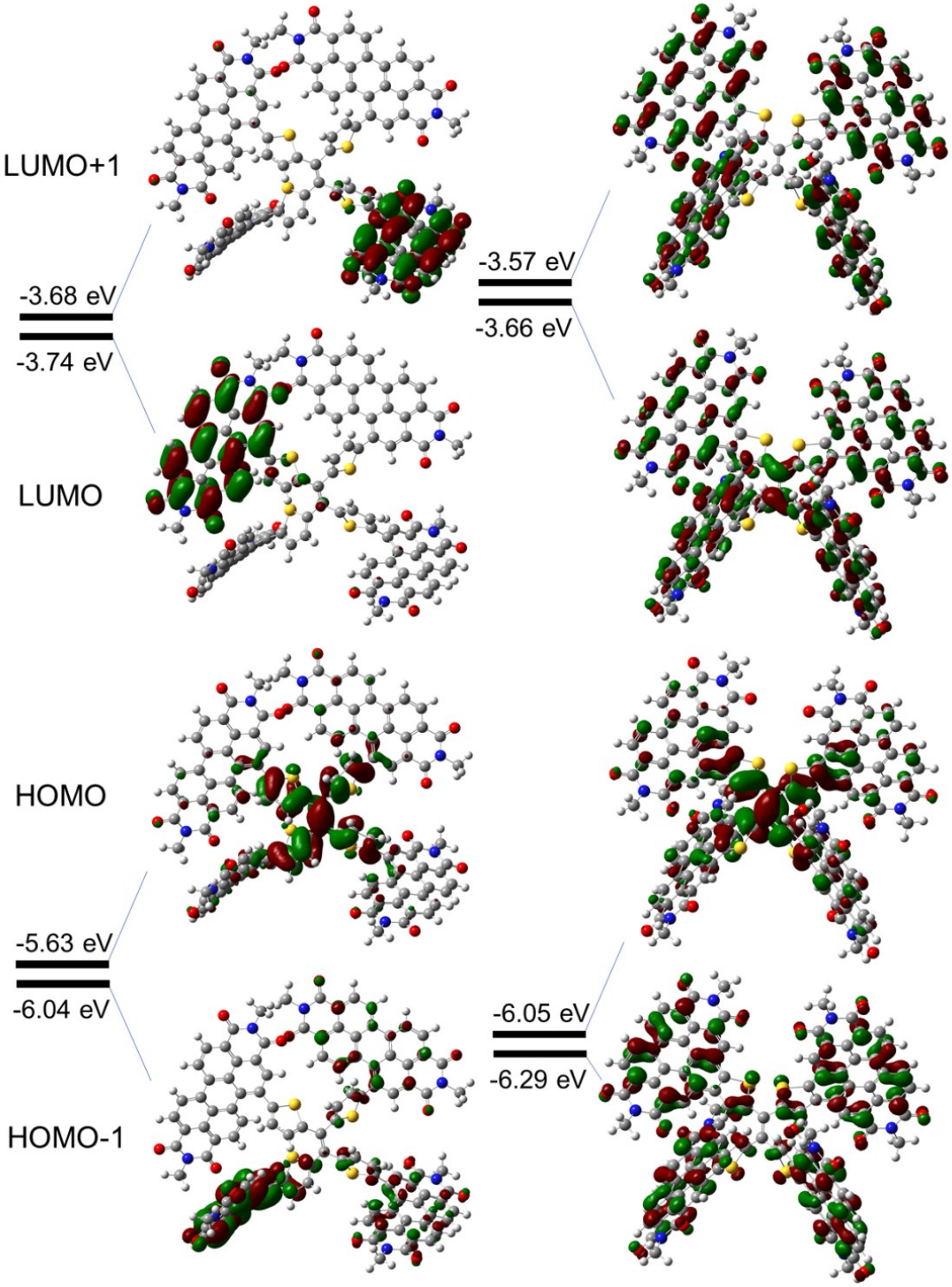


Fig. S3 Frontier molecular orbitals (HOMO-1, HOMO, LUMO and LUMO+1) of TTE-PDI4 (left) and FTTE-PDI4 (right).

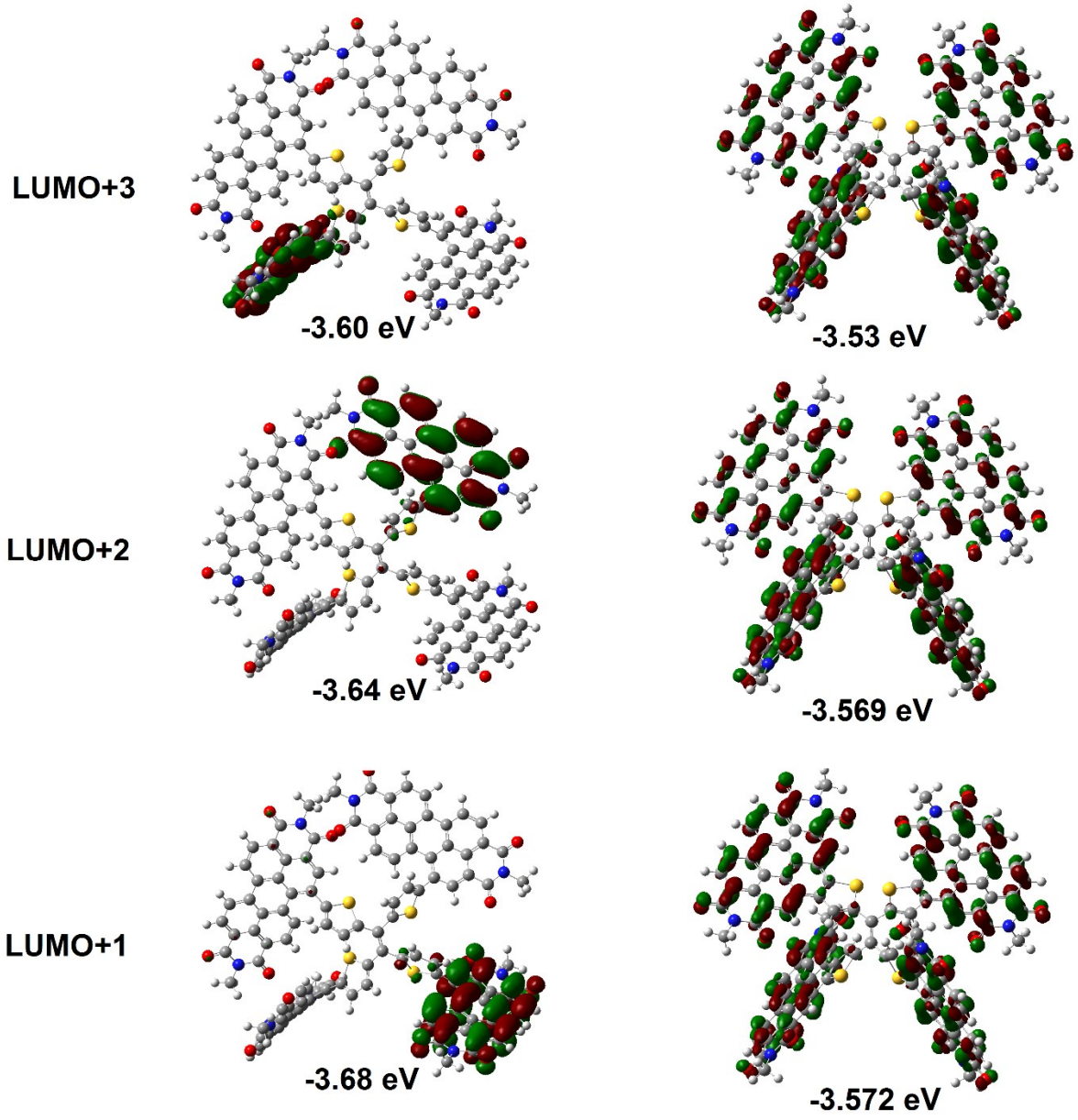


Fig. S4 Frontier molecular orbitals (LUMO+1 to LUMO +3) of TTE-PDI4 (left) and FTTE-PDI4 (right).

TTE-PDI

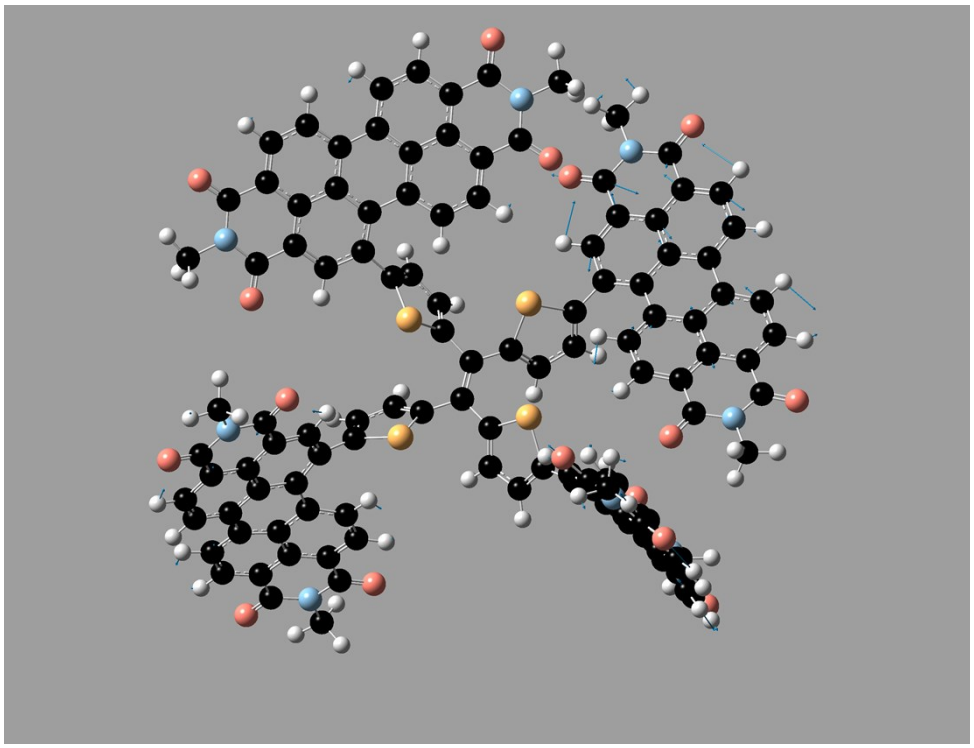

FTTE-PDI

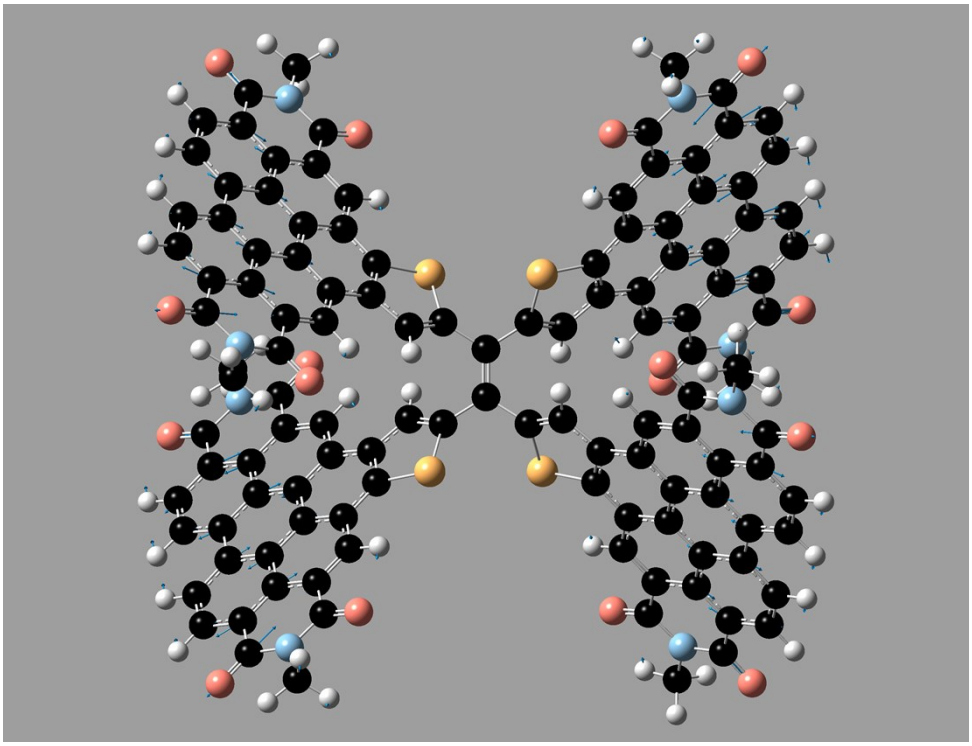

Fig. S5 Chemical structures of the two molecules with arrows indicating the vibrational movements of the atoms, showing the strong C=C bond stretch n FTTE-PDI4.

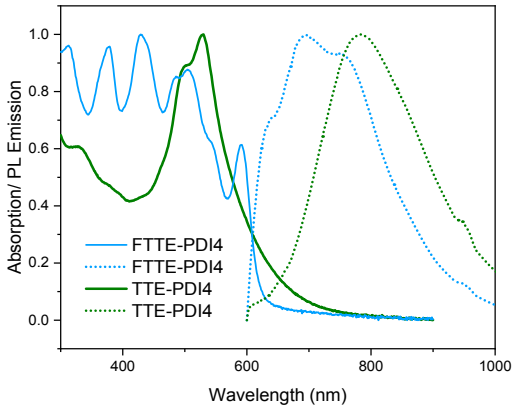


Fig. S6 Photoluminescence measurements (dotted lines) of the pristine acceptors, excited at 550 nm), plotted together with the absorption of the pristine materials in film. The intersection of the absorption and emission spectra can be interpreted as the bandgap of the materials, which are calculated as 1.90 eV and 2.04 for TTE-PDI and FTTE-PDI, respectively.

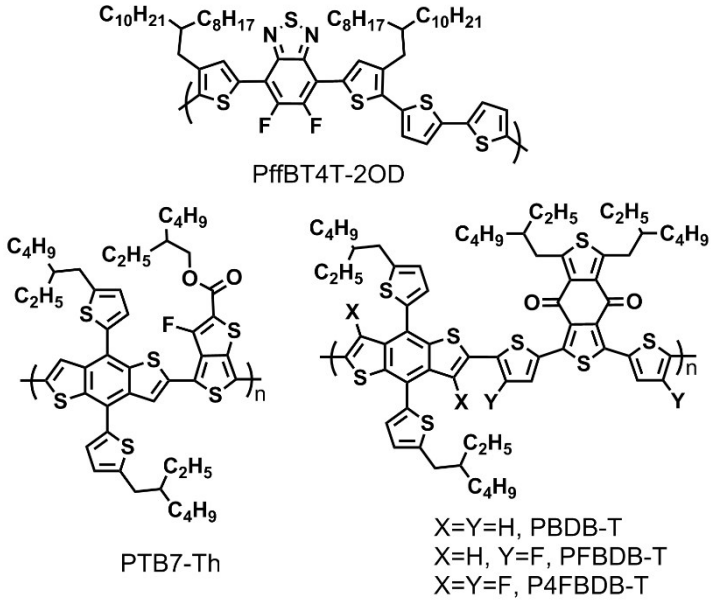


Fig. S7 Molecular structures of five polymer donors used in OPV fabrication in this work.

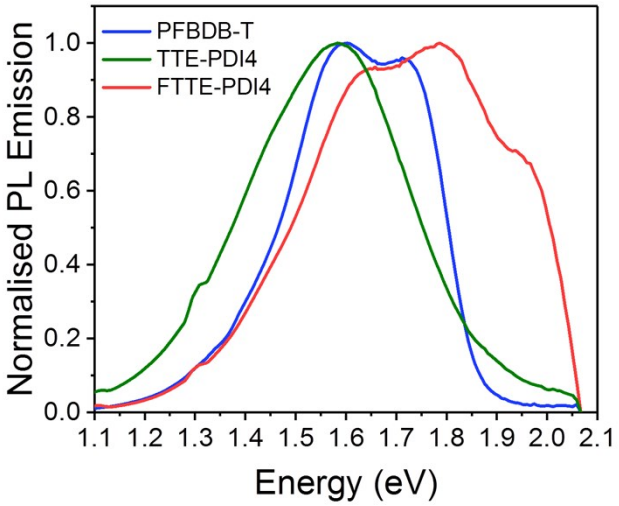


Fig. S8 Normalized photoluminescence spectra of the pristine donor and the two acceptors. FTTEE-PDI4 shows a much broader emission spectrum than TTE-PDI4, which is in agreement with its broad and oscillating absorption spectrum in film.

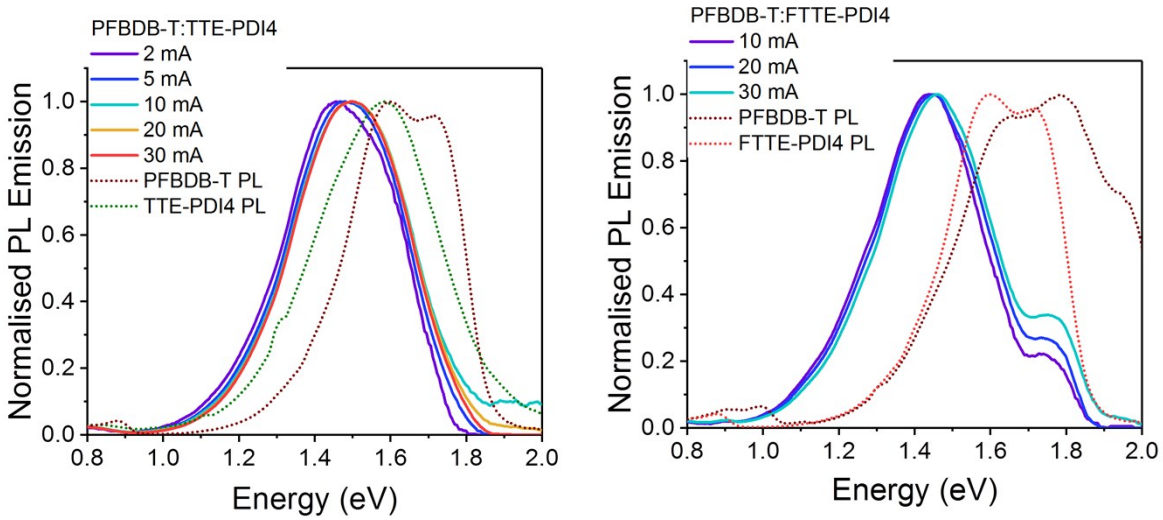


Fig. S9 Electroluminescence spectra at different injection currents for the two blends, along with the PL spectra of the pristine donor and acceptor. In both cases, the peak EL emission is strongly redshifted from the emission of the pristine materials, indicating that it originates from CT-state emission. The spectra are weakly dependent on the injection current in both blends. We note that there is some contribution to the EL emission from the FTTEE-PDI4 singlet emission in the PFBDB-T:FTTE-PDI4 blend, suggestive of strong aggregation in that blend.

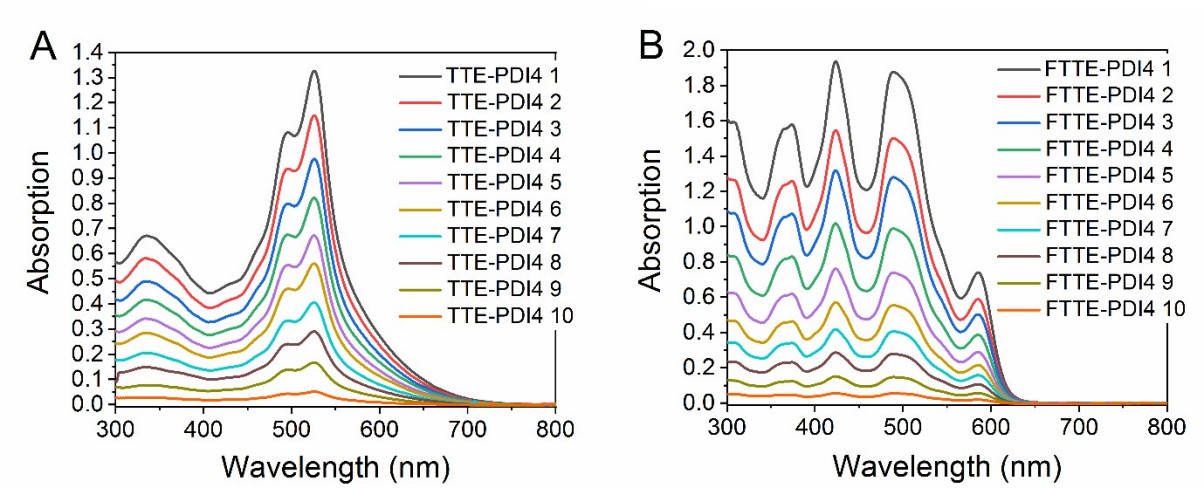


Fig. S10 Absorption spectra of TTE-PDI4 (A) and FTTB-PDI4 (B) in chloroform with various solution concentrations, started at $1.1 \times 10^{-5}$ and $1.3 \times 10^{-5}$ mol $L^{-1}$ respectively.

Table S1 Device parameters of TTE-PDI4 and FTTE-PDI4 under different processing conditions.

| Donor | Acceptor | Ratio | Additive | Annealing | $J_{SC}$ (mA $cm^{-2}$) | $V_{OC}$ (V) | FF | PCE (%) |
|---|---|---|---|---|---|---|---|---|
| PTB7-Th | FTTE-PDI4 | 1:1.5 | 2% DIO | | 11.20 | 0.89 | 0.47 | 4.6 |
| PffBT4T-2OD | FTTE-PDI4 | 1:1.5 | 2% DIO | | 9.35 | 0.89 | 0.44 | 3.7 |
| PBDB-T | FTTE-PDI4 | 1:1.5 | 2% DIO | | 9.50 | 0.90 | 0.58 | 5.0 |
| PFBDB-T | FTTE-PDI4 | 1:15 | 2% DIO | | 8.60 | 1.01 | 0.60 | 5.2 |
| P4FBDB-T | FTTE-PDI4 | 1:1.5 | 2% DIO | | 6.90 | 1.08 | 0.47 | 3.5 |
| PFBDB-T | FTTE-PDI4 | 1:1.5 | 2% CN | | 8.45 | 1.01 | 0.62 | 5.3 |
| PFBDB-T | FTTE-PDI4 | 1:1.5 | | | 8.20 | 1.01 | 0.64 | 5.3 |
| PFBDB-T | FTTE-PDI4 | 1:2 | 2% CN | | 8.81 | 1.01 | 0.63 | 5.6 |
| PFBDB-T | FTTE-PDI4 | 1:2 | | | 8.87 | 1.02 | 0.63 | 5.7 |
| PFBDB-T | FTTE-PDI4 | 1:2 | 2% CN | 140 | 10.85 | 1.00 | 0.59 | 6.4 |
| PFBDB-T | FTTE-PDI4 | 1:2 | | 140 | 8.26 | 1.01 | 0.60 | 5.0 |
| PFBDB-T | FTTE-PDI4 | 1:1 | | | 7.46 | 0.99 | 0.47 | 3.5 |
| PFBDB-T | TTE-PDI4 | 1:1 | 2% CN | | 6.88 | 0.99 | 0.51 | 3.5 |
| PFBDB-T | TTE-PDI4 | 1:5 | 2% CN | | 7.3 | 1.00 | 0.50 | 3.6 |
| PFBDB-T | TTE-PDI4 | 1:2 | 2% CN | | 5.38 | 0.93 | 0.43 | 2.1 |
| PFBDB-T | TTE-PDI4 | 1:1.5 | | | 6.98 | 0.99 | 0.51 | 3.5 |
| PFBDB-T | TTE-PDI4 | 1:1.5 | | 140 | 7.43 | 0.99 | 0.51 | 3.8 |
| PFBDB-T | TTE-PDI4 | 1:1.5 | 2% CN | 140 | 6.46 | 1.01 | 0.53 | 3.5 |

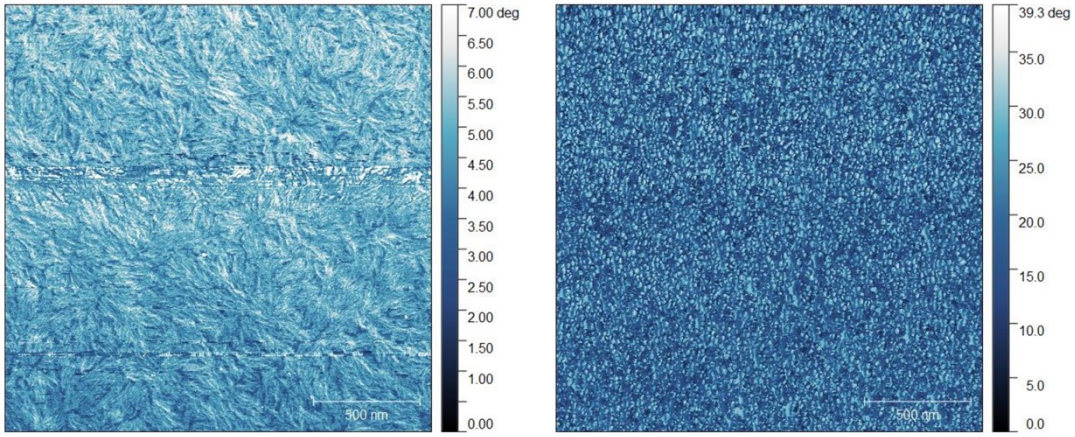


Fig. S11 AFM phase images (2 μm × 2 μm) of the PFBDB-T:TTE-PDI4 (left) and PFBDB-T:FTTE-PDI4 (right) blend films.

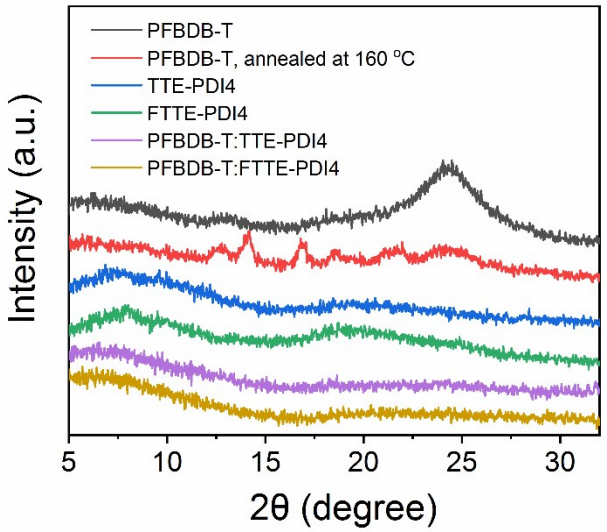


Fig. S12 XRD curves of PFBDB-T (w/o annealing), TTE-PDI4, FTTE-PDI4, and the optimal blend films based on PFBDB-T:TTE-PDI4 and PFBDB-T:FTTE-PDI4. All the thin films were drop-casted from chlorobenzene solutions on Si substrates.

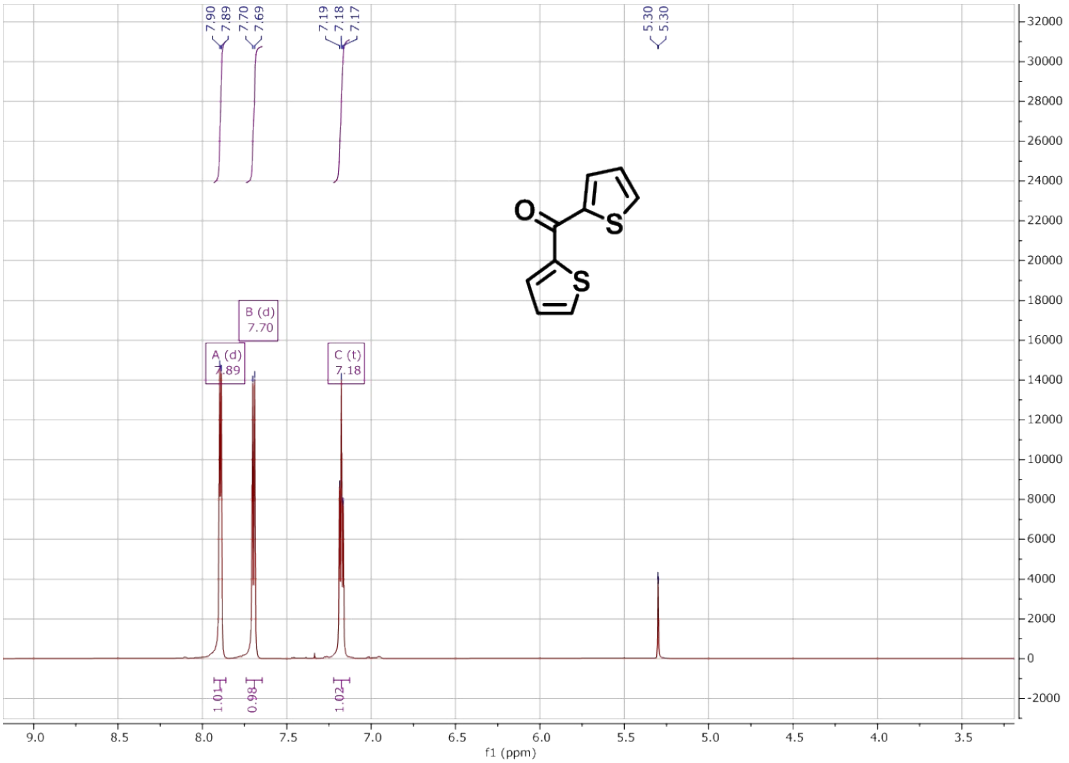


Fig. S13 $^{1}H$ NMR spectrum of DTK in $CDCl_3$.

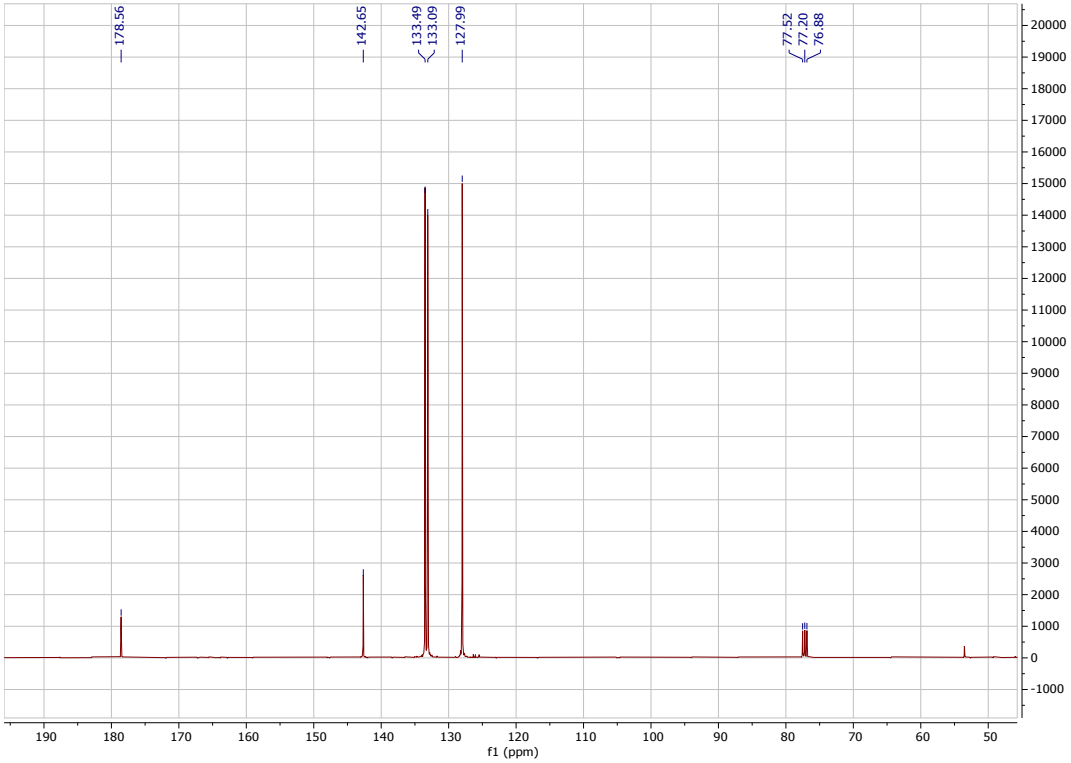


Fig. S14 $^{13}C$ NMR spectrum of DTK in $CDCl_3$.

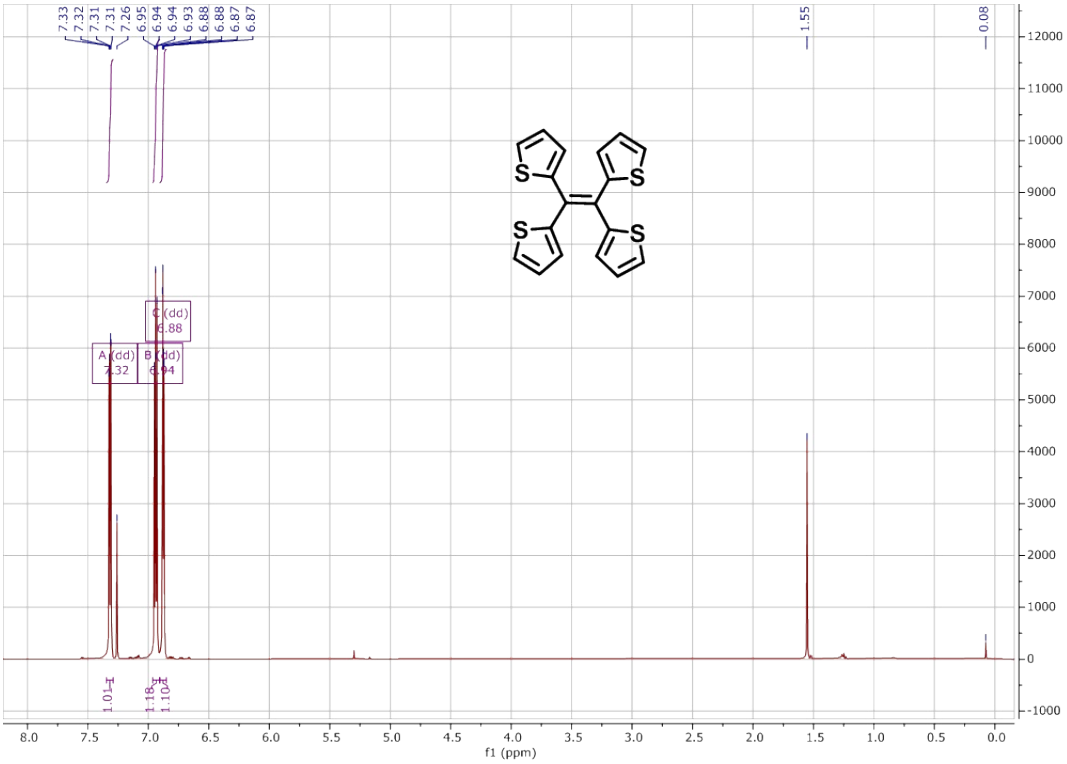


Fig. S15 $^{1}H$ NMR spectrum of TTE in $CDCl_3$.

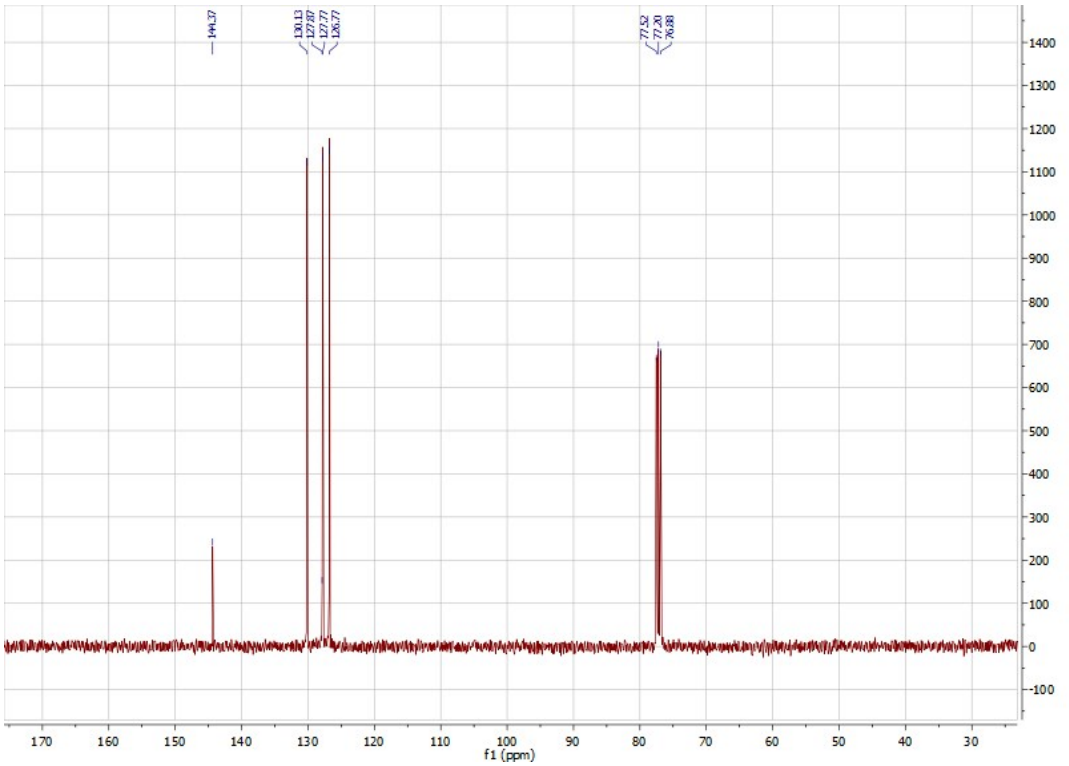


Fig. S16 $^{13}C$ NMR spectrum of TTE in $CDCl_3$.

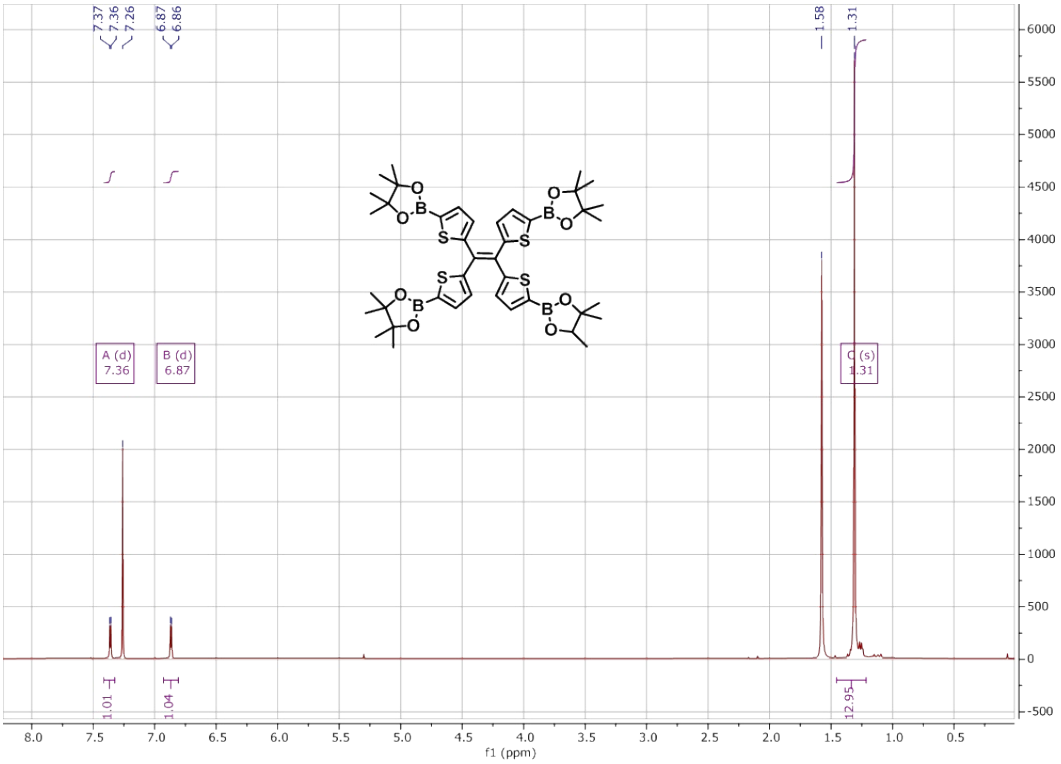


Fig. S17 $^{1}H$ NMR spectrum of TTE-Bpin4 in $CDCl_3$.

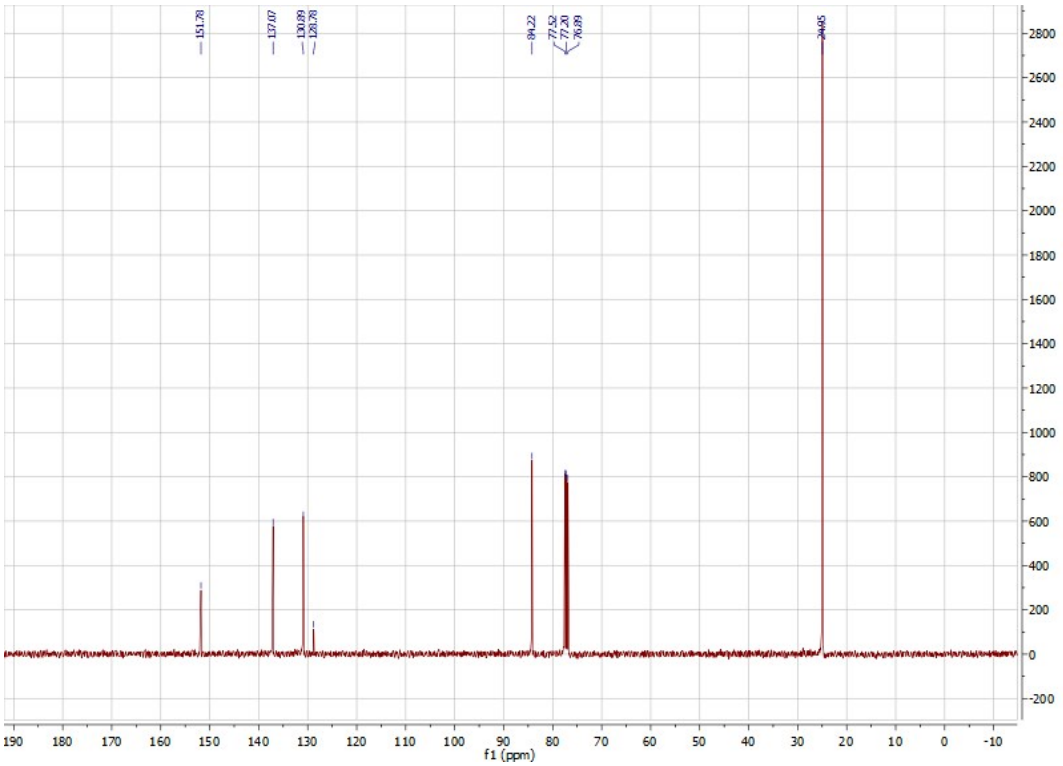


Fig. S18 $^{13}C$ NMR spectrum of TTE-Bpin4 in $CDCl_3$.

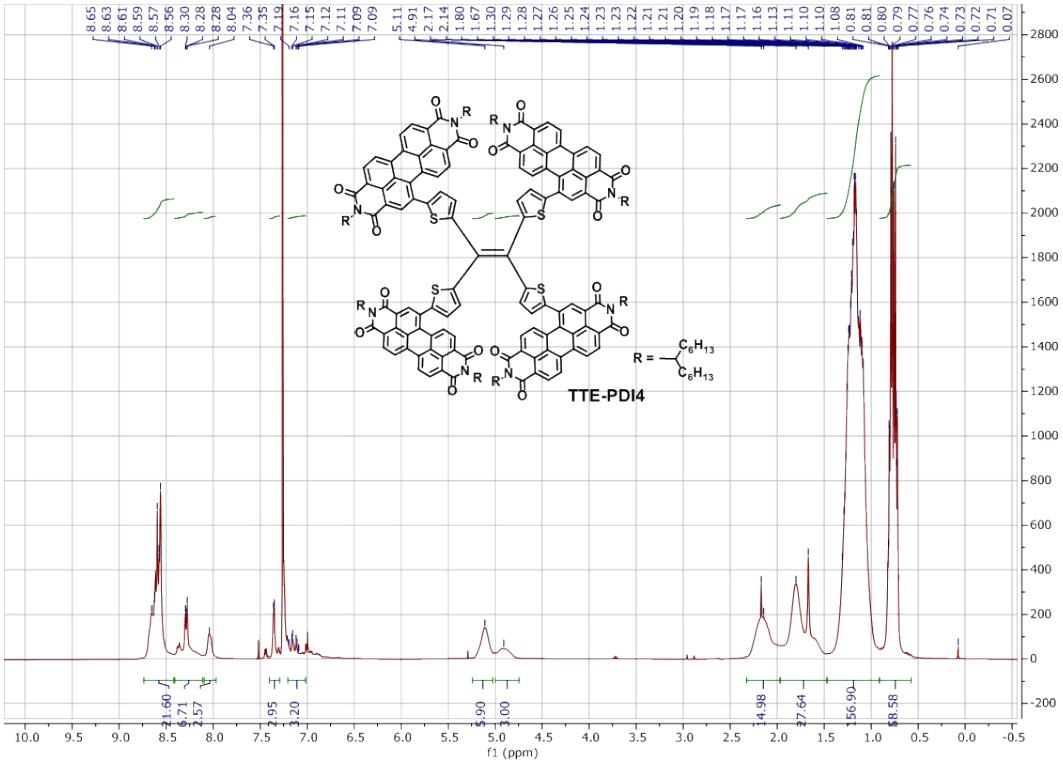


Fig. S19 $^{1}$H NMR spectrum of TTE-PDI4 in $CDCl_3$.

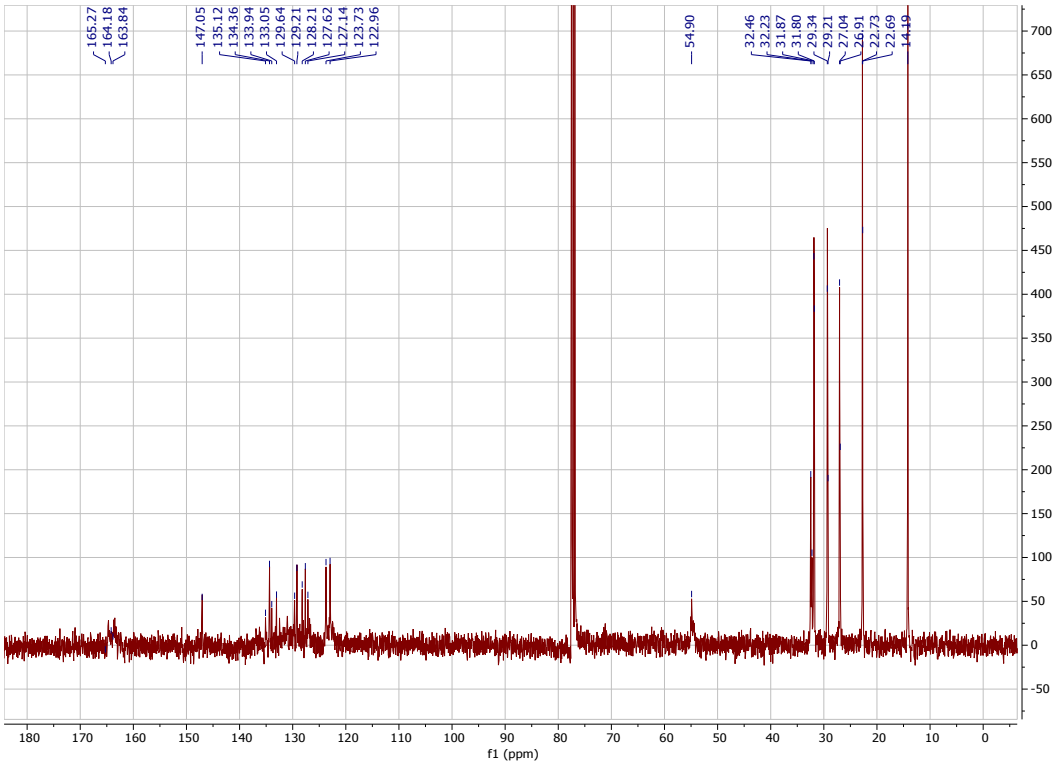


Fig. S20 $^{13}$C NMR spectrum of TTE-PDI4 in $CDCl_3$.

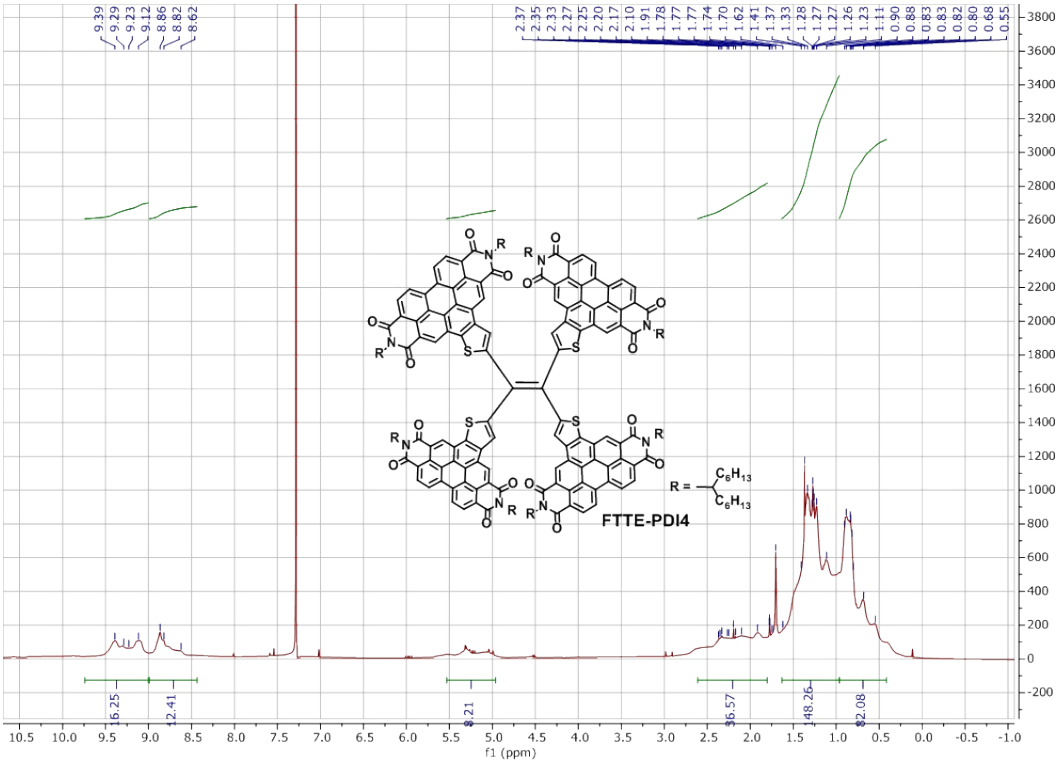


Fig. S21 $^{1}H$ NMR spectrum of FTTE-PDI4 in $CDCl_3$.

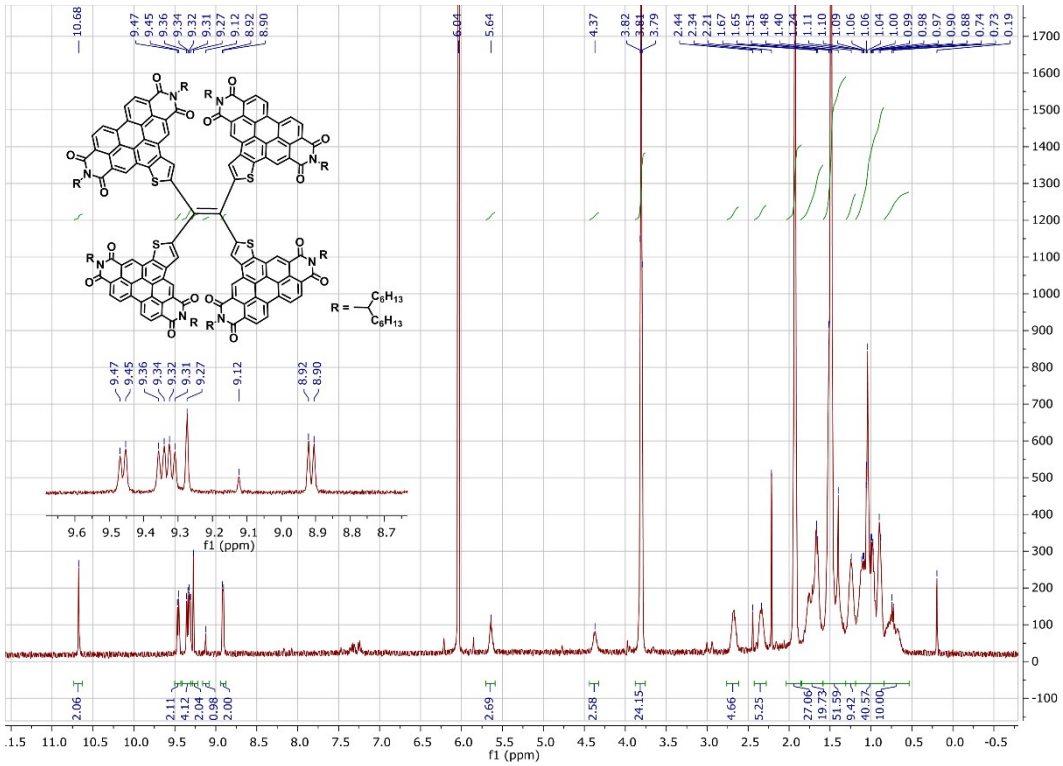


Fig. S22 $^{1}H$ NMR spectrum of FTTE-PDI4 in d2-tetrachloroethane at 120 °C.

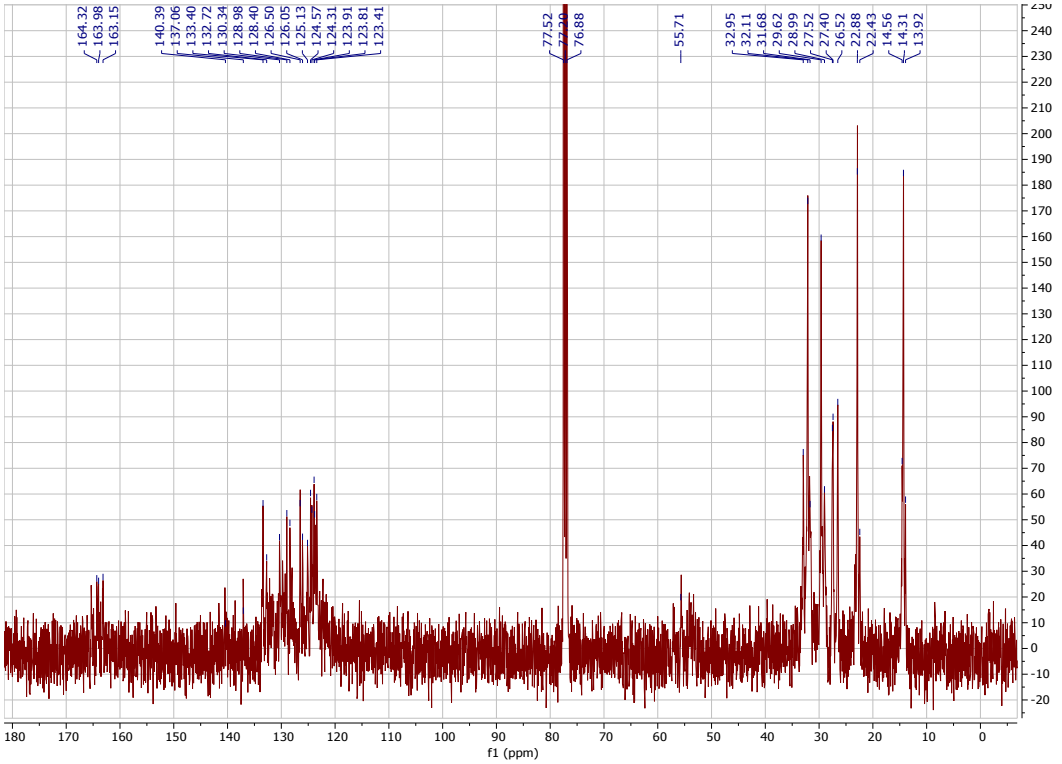


Fig. S23 $^{13}C$ NMR spectrum of FTTE-PDI4 in $CDCl_3$.

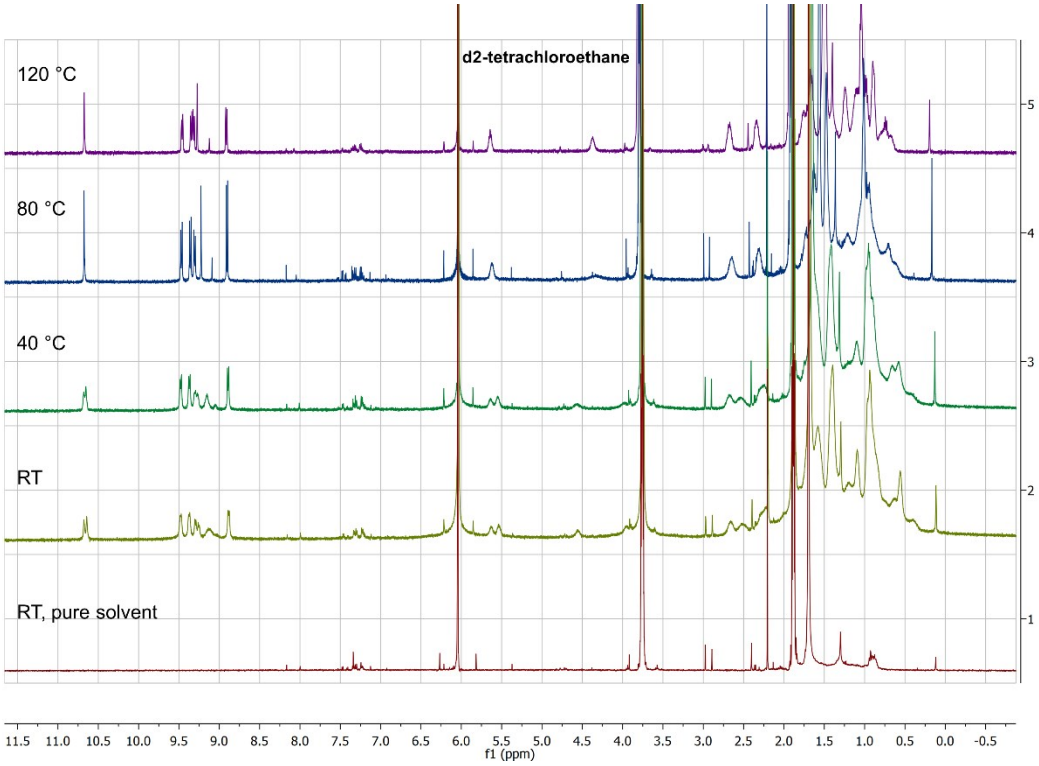


Fig. S24 Variable temperature $^{1}H$ NMR spectra of FTTE-PDI4 in d2-tetrachloroethane. Note that the bottom spectra is that of the solvent, d2-tetrachloroethane as purchased (after several months of shelf storage), and shows clear signs of impurities and degradation.

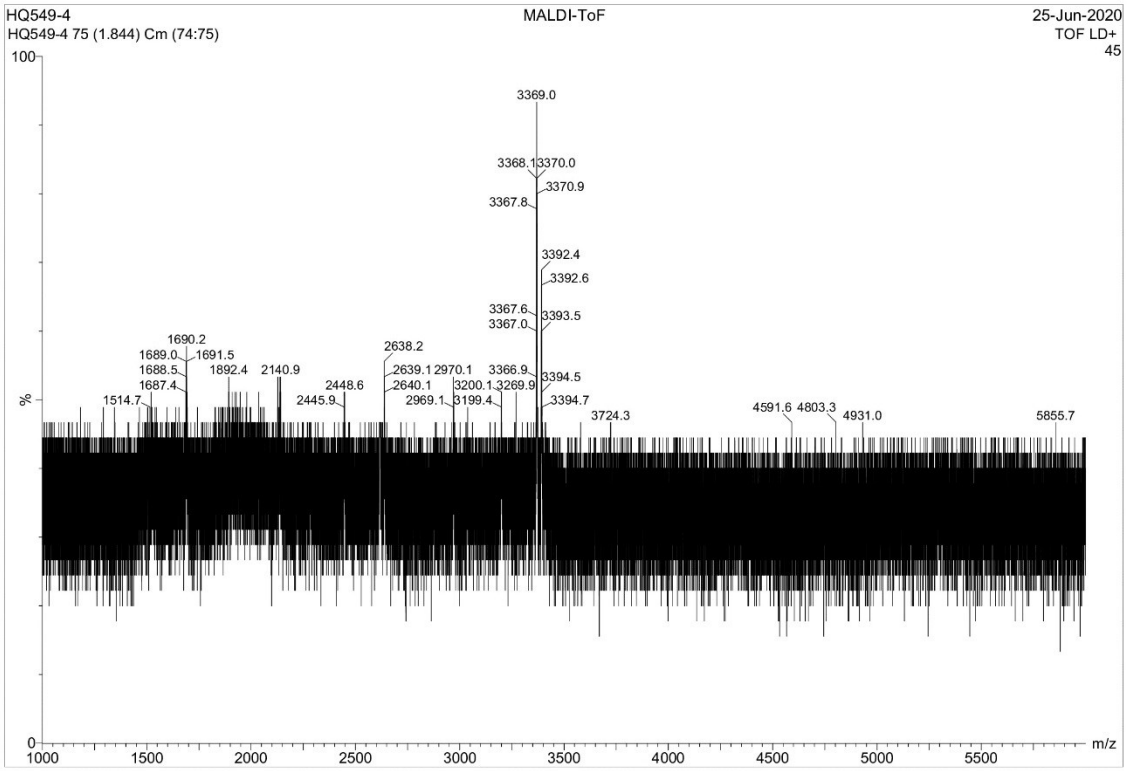


Fig. S25 MALDI-TOF MS plot of TTE-PDI4.

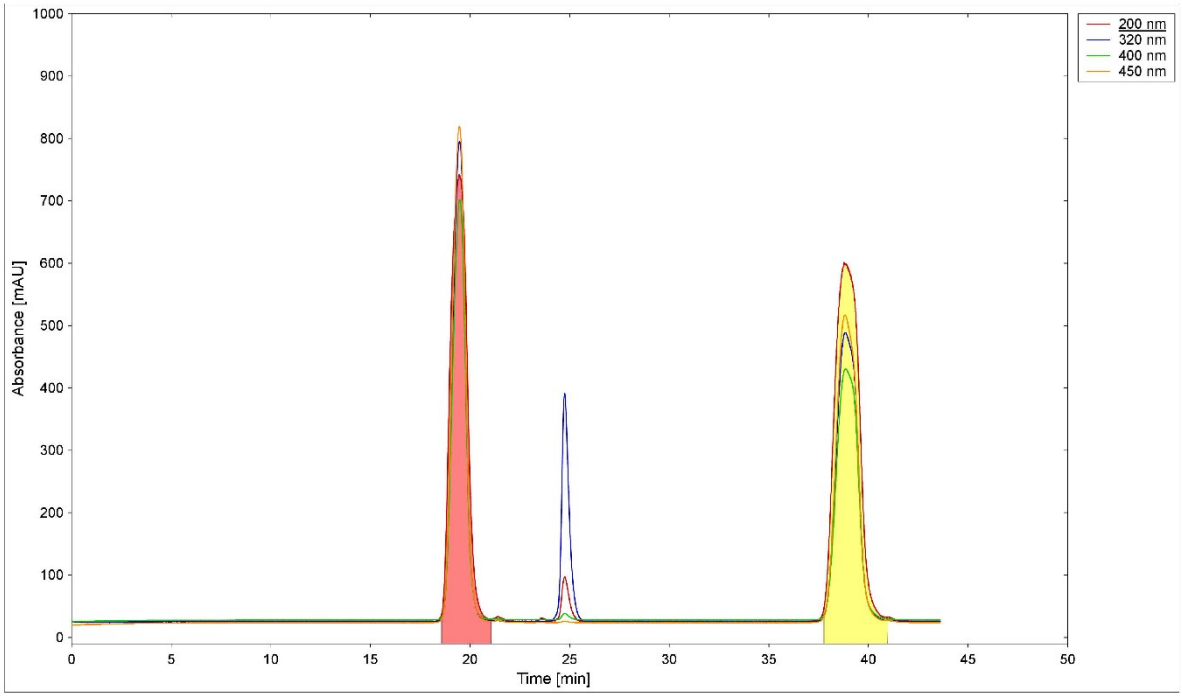


Fig. S26 Recycling GPC UV-Vis trace of TTE-PDI4. The peak at 38-40 minutes was collected.

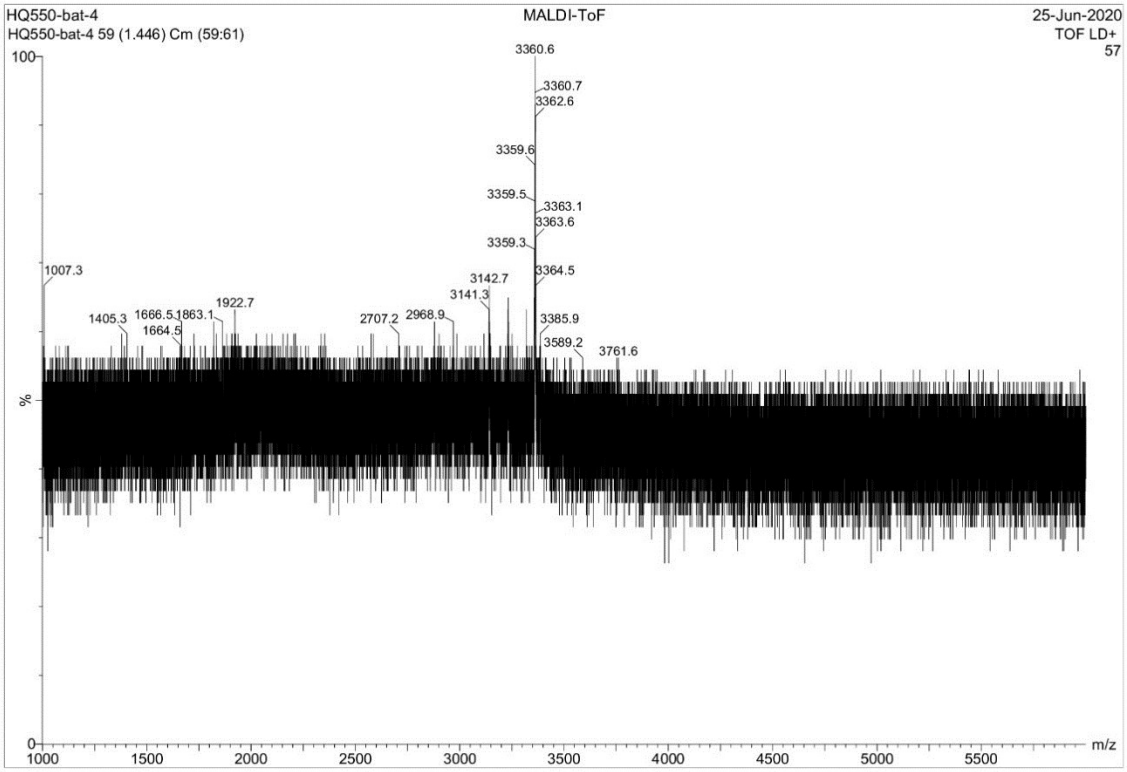


Fig. S27 MALDI-TOF MS plot of FTTE-PDI4.

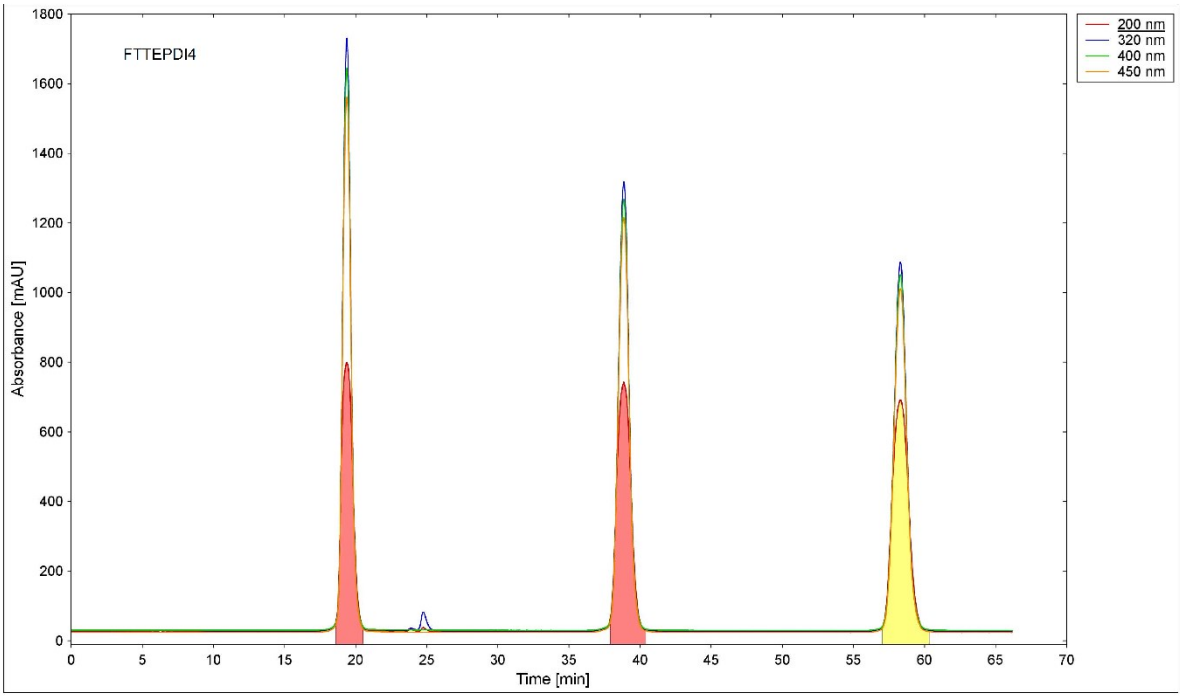


Fig. S28 Recycling GPC UV-Vis trace of FTTE-PDI4. The peak at 58-60 min was collected.

1. Y. Liu, J. Zhao, Z. Li, C. Mu, W. Ma, H. Hu, K. Jiang, H. Lin, H. Ade and H. Yan, *Nat. Commun.*, 2014, **5**, 5293.
2. D. Qian, L. Ye, M. Zhang, Y. Liang, L. Li, Y. Huang, X. Guo, S. Zhang, Z. a. Tan and J. Hou, *Macromolecules*, 2012, **45**, 9611-9617.
3. Z. Fei, F. D. Eisner, X. Jiao, M. Azzouzi, J. A. Röhr, Y. Han, M. Shahid, A. S. R. Chesman, C. D. Easton, C. R. McNeill, T. D. Anthopoulos, J. Nelson and M. Heeney, *Adv. Mater.*, 2018, **30**, 1705209.
4. F. D. Eisner, M. Azzouzi, Z. Fei, X. Hou, T. D. Anthopoulos, T. J. S. Dennis, M. Heeney and J. Nelson, *J. Am. Chem. Soc.*, 2019.
5. M. J. Frisch, G. W. Trucks, H. B. Schlegel and M. A. R. G. E. Scuseria, J. R. Cheeseman, G. Scalmani, V. Barone, G. A. Petersson, H. Nakatsuji, X. Li, M. Caricato, A. Marenich, J. Bloino, B. G. Janesko, R. Gomperts, B. Mennucci, H. P. Hratchian, J. V. Ortiz, A. F. Izmaylov, J. L. Sonnenberg, D. Williams-Young, F. Ding, F. Lipparini, F. Egidi, J. Goings, B. Peng, A. Petrone, T. Henderson, D. Ranasinghe, V. G. Zakrzewski, J. Gao, N. Rega, G. Zheng, W. Liang, M. Hada, M. Ehara, K. Toyota, R. Fukuda, J. Hasegawa, M. Ishida, T. Nakajima, Y. Honda, O. Kitao, H. Nakai, T. Vreven, K. Throssell, J. A. Montgomery, Jr., J. E. Peralta, F. Ogliaro, M. Bearpark, J. J. Heyd, E. Brothers, K. N. Kudin, V. N. Staroverov, T. Keith, R. Kobayashi, J. Normand, K. Raghavachari, A. Rendell, J. C. Burant, S. S. Iyengar, J. Tomasi, M. Cossi, J. M. Millam, M. Klene, C. Adamo, R. Cammi, J. W. Ochterski, R. L. Martin, K. Morokuma, O. Farkas, J. B. Foresman, and D. J. Fox, *Gaussian 09, Revision D.01, Gaussian, Inc., Wallingford CT*, 2016.
6. A. D. Becke, *J. Chem. Phys.*, 1993, **98**, 5648-5652.
7. C. Lee, W. Yang and R. G. Parr, *Phys. Rev. B*, 1988, **37**, 785-789.